RPE | Radiation Physics & Engineering
An International Peer-Reviewed Journal
Published by K.N. Toosi University of Technology
http://rpe.kntu.ac.ir
Research Article

Radiation Physics and Engineering 2022; 3(3):29–37
https://doi.org/10.22034/RPE.2022.337483.1076

Thermal-hydraulic analysis of a dry storage cask for VVER-1000 spent nuclear fuel

Mohammad Ali Hejazi[a], Seyed Khalil Mousavian[b,*], Mohammad Outokesh[a]

[a] *Department of Energy Engineering, Sharif University of Technology, P.O. Box: 11155-1639, Tehran, Iran*
[b] *Reactor and Nuclear Safety Research School, Nuclear Science & Technology Research Institute, P.O. Box: 14399-55933, Tehran, Iran*

HIGHLIGHTS

- Thermal-hydraulic analysis of dry storage cask for Bushehr nuclear power plant is performed.
- The proposed Bushehr dry storage cask is simulated by applying ANSYS CFX as a CFD tool.
- Thermal behavior of dry storage cask is improved due to using spacers and fins in cask design.

ABSTRACT

In this study, thermal-hydraulic analysis of a dry storage cask for Bushehr Nuclear Power Plant spent nuclear fuels is carried out. Geometry drawing and mesh generation were completed in SolidWorks and Gambit software, respectively. Three different cases were considered for the cask geometry and design including cask with/without spacers and cask with spacers and fins. Thermal-hydraulic analysis of the cask was performed for steady-state and normal storage conditions in ANSYS CFX solver package. Simulation results indicated a weak thermal-hydraulic behavior of the cask in the geometry without spacer and maximum fuel temperature exceeded the allowable safety limits. However, with the addition of spacers and fins in the geometry of the cask, thermal behavior of the cask was significantly improved and maximum fuel temperature achieved a proper margin compared to the allowable safety limits. As a result, the spent fuel integrity will be maintained in the normal storage conditions. The simulation results were compared with a literature published paper and it showed a good agreement between the calculated results.

KEYWORDS

Dry storage cask
Thermal-hydraulic analysis
Computational fluid dynamics
Spent nuclear fuel
Bushehr nuclear power plant

HISTORY

Received: 13 April 2022
Revised: 14 May 2022
Accepted: 03 June 2022
Published: Summer 2022

1 Introduction

Storage of the spent nuclear fuels is one of the topics of interest in recent years and many studies have been conducted on this field in order to design storage casks for spent nuclear fuels, since many spent fuel pools are reaching or have reached their full capacity and no permit has been issued to bury them in a natural depository (Rezaeian, 2016).

1.1 Overview of spent fuel storage technologies

There are two basic spent fuel storage technologies; wet and dry. Wet storage is the most common technology and is typically associated with AR (At Reactor) storages and large buffer storage for reprocessing facilities. Water provides efficient cooling and shielding after discharge. Unlike wet storage, dry storage technologies were in their infancy 30+ years ago with use being limited to the storage of some research reactor fuels and some gas cooled power reactor fuel (IAEA-TECDOC-1862, 2019).

Initially dry storage technologies were single purpose systems. They only provided AFR (Away From Reactor) storage (with one exception) without the capability or authorization for eventual transport off-site (without re-handling and reloading the fuel into transport casks). Examples of single purpose systems are: vaults; silos; and non-transportable casks (IAEA-TECDOC-1862, 2019).

With continuing development of dry storage technology, it was recognized that casks and containers for encapsulating the fuel could perform multiple functions. Dual purpose casks were developed (e.g., CASTOR® cask in Germany, or the NAC-STC in the USA), which allowed storage and transport to and from a storage facility with-

*Corresponding author: khmousavi@aeoi.org.ir

Table 1: TK-13 spent fuel storage cask characteristics (Azimfar and Kazemi, 2011).

Characteristics of spent fuel storage cask (VVR-1000 reactors)	Values
Number of spent fuel assembly	12
Weight of empty cask	100 tons
Weight of Uranium (average):	
- One fresh fuel assembly	431.6 (kg)
- One spent fuel assembly	416.0 (kg)
- Total of 12 spent fuel assembly	5000 (kg)
Height of cask (dimensions)	6000 (mm)
External diameter of cask (container jacket)	2295(mm)
Diameter of internal cavity	1225 (mm)
Thickness of steel that surround the cask	340 (mm)
Initial enrichment of fuel, relative to U-235	5% or less
Mean depth of fuel burnup	40 $MW.day.kg^{-1}.U^{-1}$
Maximum depth of fuel burnup	60 $MW.day.kg^{-1}.U^{-1}$
Time of holding in reservoir	3 Years

out re-handling the fuel assemblies. The fuel containers of some storage systems may be used for transport and/or final disposal. These are often referred to as dual or multipurpose systems, respectively (IAEA-TECDOC-1862, 2019).

1.2 Literature review

Many researches have been conducted on the topic of spent fuel storage systems and analysis of various functions of the storage casks. For example, Yoo et al. simulated TN24P cask with CFD methods using FLUENT software (Yoo et al., 2010). Simulation results were compared with experimental data and COBRA-SFS results. Comparison of the results indicated that temperature distribution was similar between FLUENT and COBRA-SFS, while there were differences in their velocity distribution. After conducting sensitivity studies, it was shown that the basket gap size was the most sensitive parameter in the analysis.

Rezaeian et al. proposed and investigated a dual-purpose cask design for BNPP spent fuels (Rezaeian et al., 2019). Overall dimensions of the cask were similar to Russian storage casks for VVER-1000 spent fuels but with some additional features in order to enhance heat removal from the cask. Thermal analysis of the cask indicated that maximum fuel cladding temperature did not exceed 380 °C and therefore spent fuel integrity was maintained during storage and transport conditions.

Lee et al. conducted a thermal-fluid flow analysis and demonstration test for a spent fuel storage system using FLUENT (Lee et al., 2009). Cask's design included inlet and outlet ducts for a natural cooling system. Effective thermal conductivities of a spent fuel assembly and a fuel basket were derived to optimize a thermal analysis model. Also, a porous model, which can simplify complex configuration of a fuel assembly, was used in the thermal analysis. A verified analysis model was established through a demonstration test with a half-scale model. Results showed that calculated maximum temperatures for fuel assembly and external concrete layer were below allowed limits. Therefore, thermal integrity of the cask is maintained under normal and off-normal conditions.

In the present paper, thermal-hydraulic analysis of a BNPP spent fuel storage cask via ANSYS CFX software package is described.

2 Materials and methods

2.1 BNPP spent fuel storage cask specifications

TK-13 container has been designed for transportation of 12 fuel assemblies of the WWER-1000. The frame of this container consists of a steel flask that works as a radiological shield against gamma radiation. A cylindrical layer of ethylene glycol solution (67%) has been considered for shielding against neutron radiation. The heat generated in a cask is a decay heat released as a result of radioactive decay mainly of fission products and is conducted to the outer space through conductive and radial heat removal systems. Figure 1 depicts TK-13 cask design and overall cask dimensions are presented in Table 1 (Mohammadi et al., 2017; Azimfar and Kazemi, 2011).

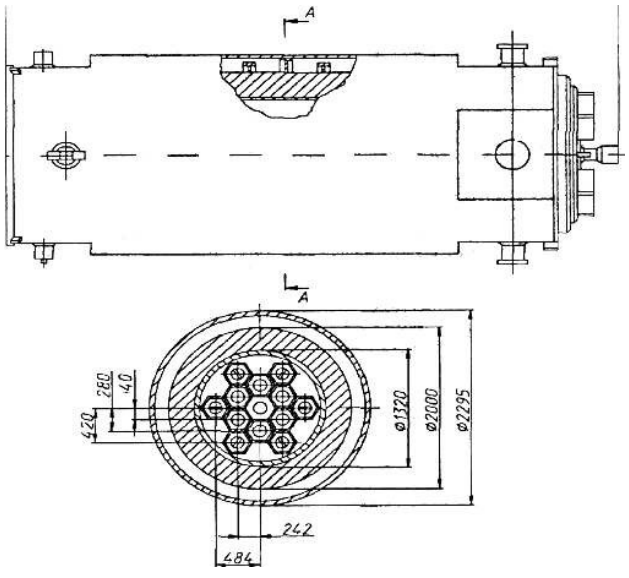

Figure 1: Transportation and storage container of spent fuel in WWER-1000 (Mohammadi et al., 2017).

Table 2: Characteristics of fuel rod and fuel assembly of WWER-1000 (Mohammadi et al., 2017).

Characteristic	Amount
Length of cross section of assembly (mm)	234
Number of fuel rods in assembly	312
Pitch between fuel rods (mm)	12.75
Number of holding nets	15
Material used in fuel rods, holding nets, control channel and central tubes (wt)	Zr (98.97%), Nb (1%), Hf (0.03%)
Inner diameter and thickness of fuel casing (mm)	9.1 and 0.69
Inner diameter and thickness of conductor channels (mm)	13.1 and 1
Inner diameter and thickness of central tube (mm)	13.1 and 1
Active length of fuel rod (mm)	3530
Initial enrichment of fuel, relative to U-235	4.4
Mass of fuel in one fuel rod (kg)	1.575

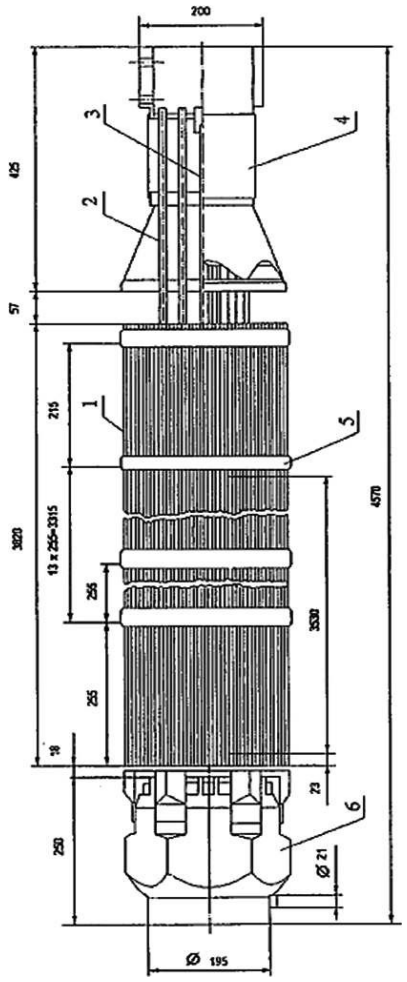

Figure 2: General view from WWER-1000 fuel assembly: 1) fuel rod, 2) guide channels, 3) central rod, 4) head of fuel assembly, 5) net, and 6) terminal part (Mohammadi et al., 2017).

2.2 BNPP spent fuel specifications

Bushehr NPP fuel assembly is shown in Fig. 2. Each assembly has a hexagonal cross-section consisting of 312 fuel rods, 18 guide channels for control rods and burnable poisons, one central channel, one channel for inter-cell interference detector (ICID) and fifteen spacing grids. Fuel pellets are made of UO_2 and are located inside a 0.65 mm thick cladding of Zr+1%Nb. Active length of the fuel assembly is 353 cm. Fuel rods' diameter is 9.1 mm and their pitch in fuel assemblys hexagonal matrix is 12.75 mm. Table 2 displays overall fuel rod and fuel assembly characteristics. Radioactivity data of BNPP spent fuel with 49 MW.day.kg^{-1}.U^{-1} burnup after 3 years of cooling period is shown in Table 3 (Rezaeian, 2016; Mohammadi et al., 2017).

Table 3: Radiation characteristics of each BNPP spent fuel assembly (Rezaeian et al., 2019).

Decay heat	Neutron radiation	Gamma radiation
2 (kW)	7×10^8 (S^{-1})	2×10^{16} (S^{-1})

2.3 Governing thermal-hydraulic equations in spent fuel dry storage casks

The main governing thermal-hydraulic equations in spent fuel casks' analysis are the continuity, momentum and energy equations:

$$\frac{\partial}{\partial x_i}(\rho u_i) = 0 \tag{1}$$

$$\frac{\partial}{\partial t}(\rho u_i)+\frac{\partial}{\partial x_j}(\rho u_i u_j) = \frac{\partial}{\partial x_j}\left[\mu\left(\frac{\partial u_i}{\partial x_j}+\frac{\partial u_j}{\partial x_i}\right)-\frac{2}{3}\left(\mu\frac{\partial u_l}{\partial x_l}\right)\right] - \frac{\partial p}{\partial x_i}+\rho g_i + F_i + \frac{\partial}{\partial x_j}(\rho\overline{u_i' u_j'}) \tag{2}$$

$$\frac{\partial}{\partial t}(\rho h)+\frac{\partial}{\partial x_i}(\rho u_i h) = \frac{\partial}{\partial x_j}(\kappa+\kappa_t)\frac{\partial T}{\partial x_i} - \frac{\partial}{\partial x_i}\sum_{j'} h_{j'} J_{j'} + \frac{Dp}{Dt}\tau_{i\kappa}\frac{\partial u_i}{\partial x_k} + S_h \tag{3}$$

where F_i represents the body force, g_i is the gravitational forces, κ_t is the turbulent conductivity due to a turbulent transport, $J_{j'}$ is the diffusion flux of species j and the source term S_h includes the heat of a chemical reaction, any interphase exchange of the heat or any other volumetric heat sources. D/Dt is a substantial derivative (Lee et al., 2009). Enthalpy h is defined as:

$$h = C_p T \tag{4}$$

where C_p is a specific heat at a constant pressure (Lee et al., 2009).

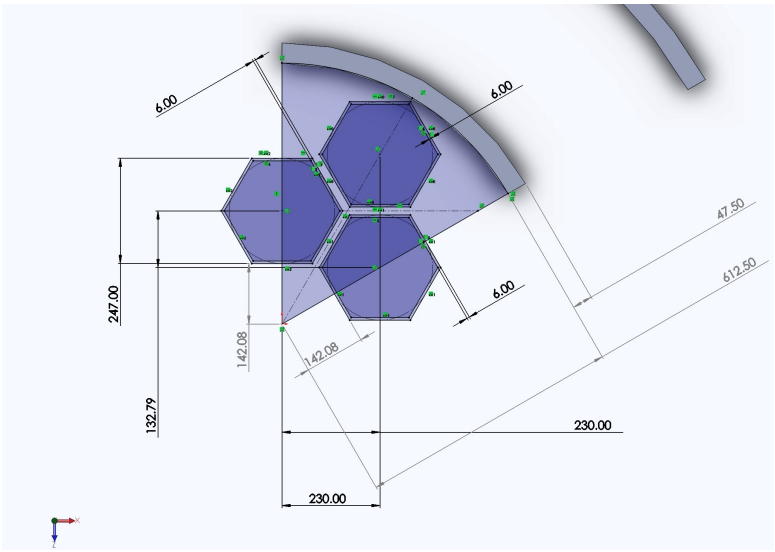

Figure 3: Sketch of the cask (Top view).

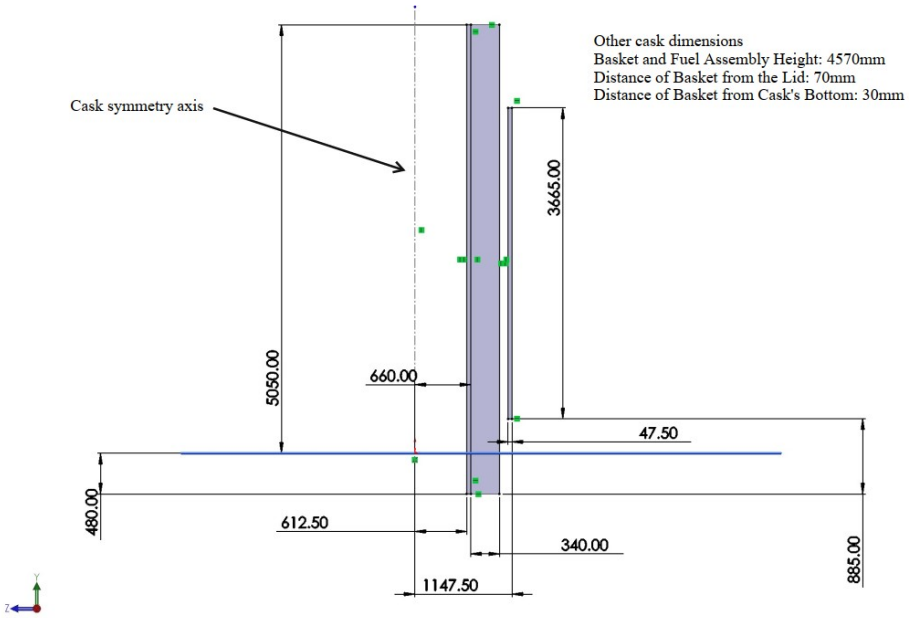

Figure 4: Sketch of the cask (side view).

Governing equations for q, convective and radiation heat transfer, at an external surface to the environment is expressed as follows:

$$q = h_{nc}A(T_s - T_a) + \sigma\varepsilon A(T_s^4 - T_a^4) \tag{5}$$

where q is heat flow (W), h is convective heat transfer coefficient (W.m^{-2}.K), A is cask surface area (m^2), T_s is temperature at cask surface (K), T_a is ambient temperature (K), σ is Stefan-Boltzmann constant (5.669×10^{-8} W.m^{-2}.K^4), and ε is emissivity of surface material (Lee et al., 2009).

Natural convection heat transfer coefficient can be derived as:

$$h_{nc} = Nu\frac{k}{L} \tag{6}$$

where $Nu = c(Gr.Pr)^2$, $Gr = g\beta(\Delta T)/v^2$, k is thermal conductivity (W.m^{-1}.K), a is exponent dependent on the flow regime, c is coefficient dependent on the flow regime and geometry, g is acceleration gravity (m.s^{-2}), L is cask length (m), β is coefficient of volumetric expansion (K^{-1}), ΔT is temperature difference between the cask surface and ambient (K), and v is dynamic viscosity (m^2.s^{-1}) (Lee et al., 2009).

2.4 Methodology

The process of performing a single CFD simulation is split into four components (ANSYS, 2019):

1. Creating the geometry/mesh
2. Defining the physics of the model
3. Solving the CFD problem
4. Visualizing the results in the postprocessor

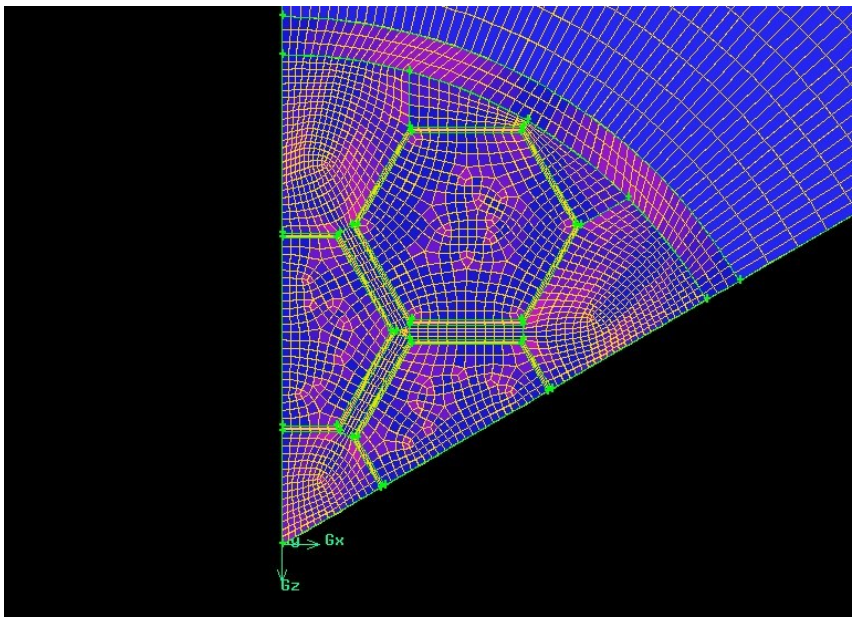

Figure 5: Top view of initial cask design's grid.

2.4.1 Geometry

Geometry of the cask was made in SolidWorks based on the dimensions of the Russian TK-13 transport cask (Mohammadi et al., 2017). For places with unknown dimensions, estimations were made based on other commercial casks. Figures 3 and 4 display cask dimensions from up and side view respectively. As shown in Fig. 3, fuel assembly and basket are connected to each other, since helium and fuel assembly region were considered as a homogeneous region. More details are explained in the physical modeling section.

2.4.2 Meshing

Structured grid with hexahedral elements was constructed for this geometry. Important grid quality parameters for initial geometry design are shown in Table 4. Cross-section for the grid is displayed in Fig. 5. According to the mesh analysis, the worst element aspect ratio, skewness, and total elements are 20.2686, 0.5715, and 471636, respectively.

It is important to note that the high aspect ratio region in the grid is mostly from the solid region, basket, and thus it will not have a significant effect on the obtained results from this grid.

Table 4: Mesh statistics for initial geometry design.

Skewness	Count	Aspect ratio	Count
0-0.1	247390	0-3	83896
0.1-0.2	120363	3-6	267489
0.2-0.3	60459	6-9	64352
0.3-0.4	34990	9-12	3323
0.4-0.5	7242	12-15	1846
0.5-0.6	1192	15-18	342
		18-21	50388

2.4.3 Physical modeling

Decay heat of spent fuels are dissipated to the environment via conduction, convection, and radiation heat transfer. For casks stored in an open space and during casks transportation, solar radiation from the Sun is also considered (Rezaeian, 2016).

Spent fuel heat transfer inside the cask and its related phenomena such as expansion of various parts and pressure changes inside the cask are very complex. Of such complexities, there is the heat transfer inside spent fuel pellet and rod which in addition to becoming porous, they are also fractured and the composition of gases inside the rod is changing. Due to such complexities in the heat transfer phenomena of spent fuel inside the cask, complete modelling of the cask is not easily achievable and simplification in various phenomena is inevitable. It is because of such complexities that experimental analysis is essential in this field (Rezaeian, 2016). Physical models applied are as follows.

The region containing spent fuel assembly and helium is considered as a homogeneous solid. Properties of this region are an average of all the constituent materials. In order to model the thermal behavior of this region, an effective thermal conductivity was defined which represents all the heat transfer phenomena occurring in that region. This parameter was defined as a temperature dependent equation (Bahney and Lotz, 1996; NUREG-2152, 2013):

$$k_{\text{eff}} = -6.455E-08 \times T^3 + 9.52E-05 \times T^2 - 0.04319 \times T + 7.601 \quad \text{(Radial)} \tag{7}$$

$$k_{\text{eff}} = 4.077E-08 \times T^3 - 8.616E-05 \times T^2 + 0.0523 \times T - 3.849 \quad \text{(Axial)} \tag{8}$$

Decay heat source of 2 kW was defined for a complete fuel assembly. Obviously, half of this value was implemented for half fuel assemblies in $\frac{1}{6}$ section of the cask.

Helium inside the cavity was modeled as an ideal gas with the kinetic theory model applied for thermal conductivity (NUREG-2152, 2013). Buoyancy model was applied in order to simulate natural convection of the gas and turbulent $k-\varepsilon$ model was selected for helium flow inside the cavity.

Boundary conditions

Symmetry boundary condition was applied for side faces of the $\frac{1}{6}$ section of geometry in order to reduce computational load of the simulation. Outer surfaces of the cask were modeled using combined heat transfer coefficient (radiation and convection) with an ambient temperature of 38 °C (Rezaeian et al., 2019). Solar radiation was implemented for the outer surfaces of the cask with heat fluxes equal to 400 W.m^{-2} and 800 W.m^{-2} for vertical and horizontal surfaces, respectively (Commission et al., 2010). An equivalent heat transfer coefficient was used for bottom of the cask, 0.17 W.m^{-2}.K, which is equivalent of conduction heat transfer in 3 m of soil (15 °C) (NUREG-2152, 2013).

2.4.4 Simulation scenarios

In order to investigate the effect of spacers and fins on thermal performance of the cask, simulations are conducted in three scenarios: cask with/without spacers and cask with spacers and fins. Moreover, due to ANSYS CFX's lack of anisotropic thermal conductivity option in material definition, simulations were conducted separately for radial and axial keff input (for fuel region) and their average (only for third scenario).

3 Results and discussions

Before discussing the results of the simulations, it is important to note that the x-axis values for temperature distributions through half fuel assembly, Z[m], are negative (Z[m] represents the radius of the cask). Negative values shown for Z[m] is due to the method in which cask's geometry was drawn. $\frac{1}{6}$ section of the cask was drawn in the negative region of the z-axis with one of the symmetry faces being on the negative side of the z-axis line. Therefore, temperature distributions through half fuel assembly go from right to left, starting from 0 to the negative value of cask's total radius.

3.1 First scenario

Radial temperature distribution of the simulated storage cask through half fuel assembly is illustrated in Fig. 6. Maximum temperature in the figure indicate that the first scenario configuration is unable to keep fuel region (fuel cladding) temperatures within allowed limits (380 °C/653.15 K) and therefore is unable to maintain fuel integrity during storage period.

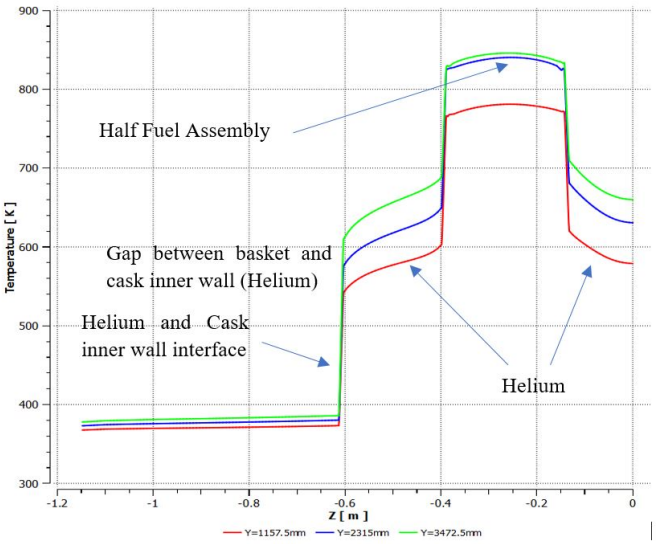

Figure 6: Temperature distribution for 1st scenario through half fuel assembly.

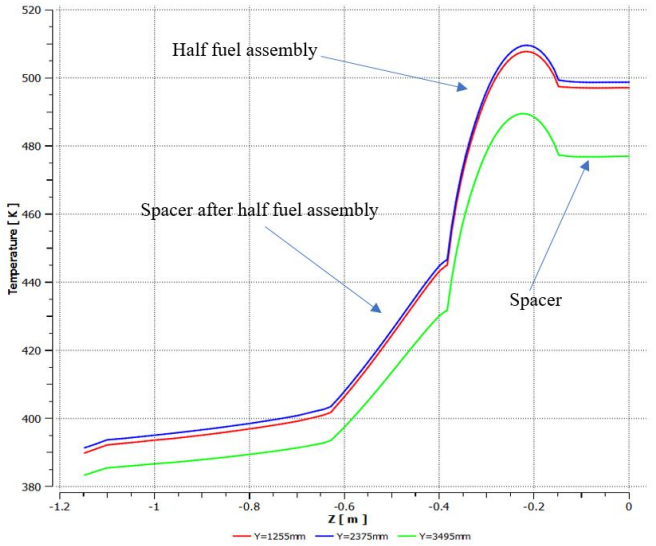

Figure 7: Temperature distribution for 2nd scenario through half fuel assembly.

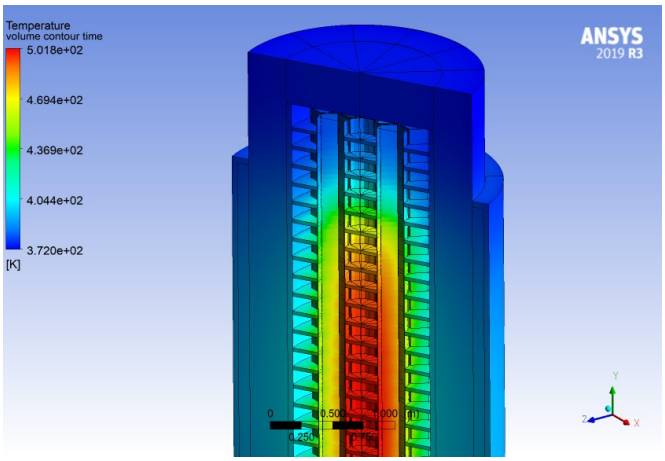

Figure 8: Temperature contour for 2nd scenario.

3.2 Second scenario

28 spacers with 3 cm thickness are added to design of the cask inside cavity in order to enhance the thermal performance of the cask. Calculated radial temperature distribution through half fuel assembly and temperature contour for $\frac{1}{2}$ section of the cask are displayed in Figs. 7 and 8. The results show a significant decrease in temperature values throughout the cask due to the addition of spacers into cask design. Maximum temperature in fuel region has fallen below safety temperature limits and by a sizeable margin. This result shows that the addition of spacers has enhanced the heat distribution inside the cask and thus significantly reduced maximum temperatures of the cask. Therefore, fuel integrity is maintained in this scenario.

Although cask's thermal performance has improved considerably, outside surface temperatures are slightly high. In order to reduce the temperature of the cask outside surface, fins are added to the design of the cask.

3.3 Third scenario

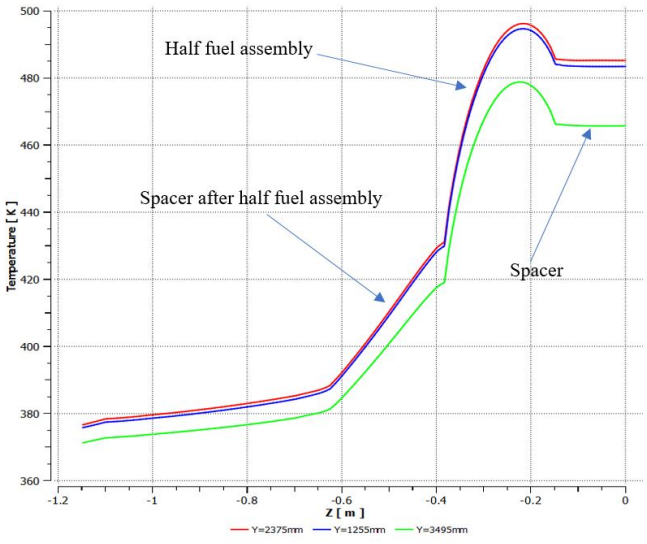

Figure 9: Temperature distribution for 3rd scenario through half fuel assembly.

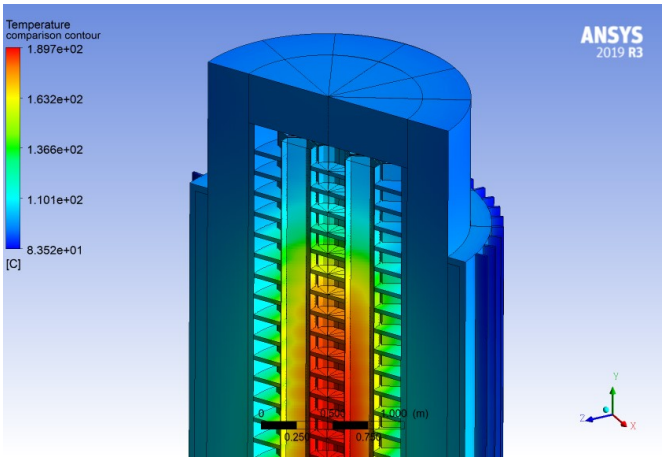

Figure 10: Temperature contour for 3rd scenario.

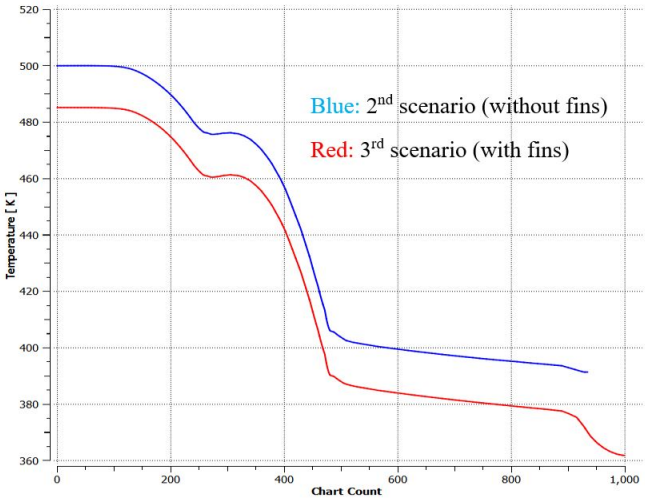

Figure 11: Comparison of radial temperature distribution through full fuel assembly for 2nd and 3rd scenario.

As seen from the above figure, addition of fins improved the thermal performance of the cask compared to second scenario. This enhanced performance affected the entire temperature distribution of the cask and reduced the temperatures of all parts of the cask.

3.4 Grid sensitivity analysis

In order to verify the results obtained from the simulations, a grid sensitivity analysis was performed. Two refined grids were constructed for each scenario's initial grids. Refined meshes of the initial grid shown in meshing section were constructed for the purpose of sensitivity analysis. Table 5 displays overall stats of the refined grids and the initial grids for first and second scenarios:

Simulations were conducted for the refined grids by implementing the same physical models, initial, and boundary conditions as the initial grids. Due to grid similarity between second and third scenario, this analysis was only performed for second scenario. Figures 12 and 13 display the comparison of results between the initial and refined grids for the first and second scenario, respectively.

Table 5: Overall stats for initial and refined grids.

	Initial grid	Refinement level 1	Refinement level 2
Total elements (1st scenario)	471636	842803	1880310
Total elements (2nd scenario)	635724	1302145	2235590

Table 6: Comparison of calculated temperatures for different cask parts during normal storage conditions between 3rd scenario and Rezaeian et al. (Rezaeian et al., 2019) results.

Location	Maximum calculated temperatures (°C)				Maximum allowed temperature (°C) (Rezaeian et al., 2019)
	3rd scenario (average k_{eff})	3rd scenario (axial k_{eff})	3rd scenario (radial k_{eff})	(Rezaeian et al., 2019)	
Basket	190	184	214	189	316
Fuel assembly	191	185	224	192	380

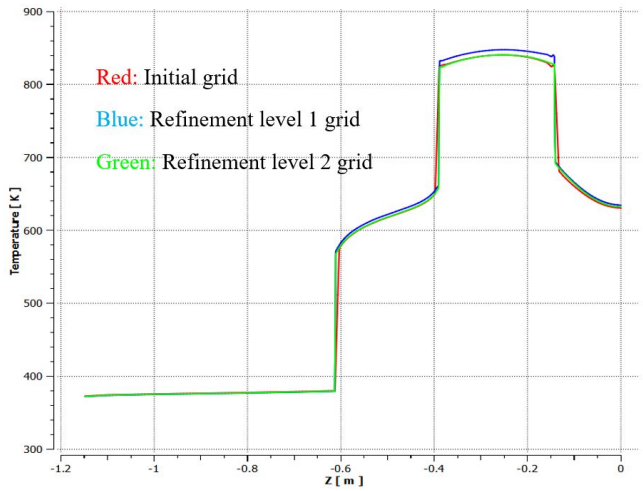

Figure 12: Comparison of results between different grids for radial temperature distribution through half fuel assembly for 1st scenario.

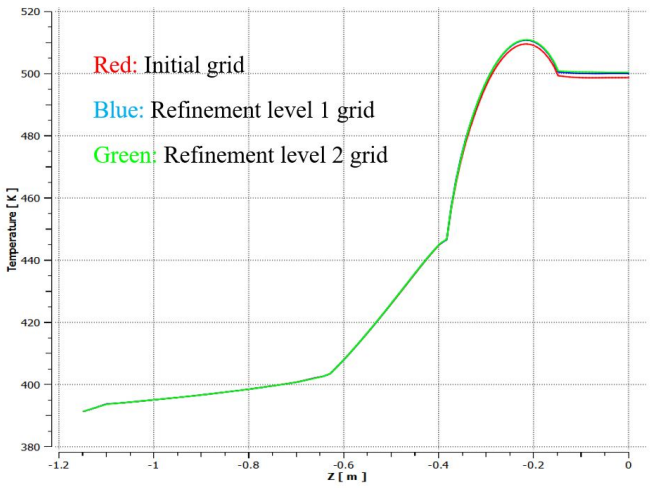

Figure 13: Comparison of results between different grids for radial temperature distribution through half fuel assembly for 2nd scenario.

As seen from the figures, grid refinements did not affect the results for various regions of the cask and similar temperature distributions were obtained for each scenario. This goes to show that the results obtained from the initial grids for all scenarios had negligible difference compared to the results from refined grids. This means that the results obtained for each scenario are independent from their respective grids and therefore grid sensitivity analysis has been accomplished.

3.5 Validation studies

Due to difficulties in obtaining required experimental apparatus in order to perform validation studies, a result comparison with other studies, with a similar cask design, was performed. Only citable study available about Russian casks' simulation was Rezaeian et. al. about localization of Russian casks for BNPP spent fuels (Rezaeian et al., 2019). Since the results of the third scenario displayed the best thermal performance among all scenarios, they were chosen to be compared with the results of Rezaeian et. al. study, which simulated a similar spent fuel assembly and cask design. It is also important to note that the assumptions used in the current study are somewhat similar to the ones used in Rezaeian et. al. study as well (Rezaeian et al., 2019). For this comparison, results of third scenario for different k_{eff} inputs (radial, axial, and their average) were obtained (Table 6).

Results comparison show that the maximum temperatures for third scenario (all k_{eff} inputs) achieved a proper margin to maximum allowable temperatures. Also, maximum temperatures calculated for third scenario (mean axial and radial k_{eff}) are close to the calculations of Rezaeian et al. (Rezaeian et al., 2019) which relatively validates the obtained results in this study. However, a proper experimental analysis is required to achieve a correct validation process.

4 Conclusions

In this study, thermal-hydraulic analysis of a dry storage cask for VVER-1000 spent fuel assemblies was conducted through the usage of ANSYS CFX software package. First scenario design showed considerably high temperatures for fuel region due to poor heat removal of the cask. Addition of spacers and fins in second and third scenarios significantly enhanced heat dissipation from the cask and

thus reducing fuel region's temperatures to below the allowed limits (380°C/653 K). Therefore, 2nd and 3rd scenario cask designs are able to maintain spent fuel integrity during storage period. However, accuracy of the simulation results is dependent on the physical model applied in the fuel assembly region as well as more detailed meshing in sensitive areas (higher computational burden). Thus, enhancing physical models for fuel assembly region (e.g., porous media model) and a better mesh quality would provide a more appropriate showcase for the cask's thermal behavior. A proper experimental data is also required for accurate validation studies. Innovations of this study include the usage of the powerful CFX software package and its' various features for simulation and data extraction, and investigating the impact of spacers on thermal performance of the dry storage cask.

References

ANSYS (2019). ANSYS Inc.

Azimfar, S. and Kazemi, A. (2011). Modal analysis of spent fuel cask for WWER-IOOO reactors. *Journal of Nuclear Science and Technology*, 56.

Bahney, R. and Lotz, T. (1996). Spent nuclear fuel effective thermal conductivity report. *Prepared for the US DOE, Yucca Mountain Site Characterization Project Office by TRW Environmental Safety Systems, Inc., July*, 11.

Commission, U. N. R. et al. (2010). Licensing requirements for the independent storage of spent nuclear fuel, high-level radioactive waste, and reactor-related greater than Class C Waste. *Code of Federal Regulations, Title*, 10.

IAEA-TECDOC-1862 (2019). *Behavior of Spent Power Reactor Fuel during Storage*. PhD thesis, International Atomic Energy Agency.

Lee, J., Choi, W., Bang, K., et al. (2009). Thermal-fluid flow analysis and demonstration test of a spent fuel storage system. *Nuclear Engineering and Design*, 239(3):551–558.

Mohammadi, A., Hassanzadeh, M., and Omidvari, N. (2017). Criticality safety analysis of TK-13 cask in Bushehr nuclear power plant. *Kerntechnik*, 82(6):637–642.

NUREG-2152 (2013). Computational fluid dynamics best practice guidelines for dry cask applications. *U.S. Nuclear Regulatory Commission*, 1.

Rezaeian, M. (2016). *Thermal, and Mechanical Design of a Dual-purpose Cask for Spent (Used) Fuels of Bushehr Nuclear Power Plant*. PhD thesis, Ph. D. Thesis, Nuclear Science and Technology Research Institue.

Rezaeian, M., Kamali, J., and Ahmadi, S. (2019). Thermal evaluation of a dual purpose cask for Bushehr nuclear reactor spent fuels under normal conditions. *Journal of Nuclear Science and Technology (JONSAT)*, 40(1):81–88.

Yoo, S. H., No, H. C., Kim, H. M., et al. (2010). Full-scope simulation of a dry storage cask using computational fluid dynamics. *Nuclear Engineering and Design*, 240(12):4111–4122.